PAPER

Conformational transitions of a DNA hairpin through transition path times

Journal of Statistical Mechanics: Theory and Experiment
An IOP and SISSA journal

PAPER: Interdisciplinary statistical mechanics

Conformational transitions of a DNA hairpin through transition path times

Shivangi Sharma and Parbati Biswas[1]

Department of Chemistry, University of Delhi, Delhi 110007, India
E-mail: pbiswas@chemistry.du.ac.in

Received 26 February 2020
Accepted for publication 8 June 2020
Published 28 July 2020

Online at stacks.iop.org/JSTAT/2020/073411
https://doi.org/10.1088/1742-5468/aba0a7

Abstract. The stochastic dynamics of zipping/unzipping transition of a DNA hairpin is theoretically investigated within the framework of generalized Langevin equation in a complex cellular environment. Analytical expressions of the distributions of transition path and first passage times are derived. The results reveal that the transition path time of DNA is shorter compared to the Kramers's first passage time. Especially, the transition path time depicts an unexpected behavior as it decreases with an increase in the height of the barrier, while the first passage time reveals an exactly opposite trend. Both mean first passage time and mean transition path time increases with an increase in the complexity/viscoelasticity of the cellular environment due to the caging effect of the hairpin. Our results for the free energy landscape, probability density, transition path time distribution and the mean transition path time of the DNA hairpin are in good agreement with those obtained from experiments and other theoretical studies.

Keywords: biomolecules, stochastic processes, transition path times, DNA hairpin

Contents

[1]Author to whom correspondence should be addressed.

1742-5468/20/073411+29$33.00

1. Introduction

DNA hairpins are single stranded structures formed from self complementary base pairing of nucleotides that play significant role in the regulation of gene expression [1, 2], DNA replication and recombination [3] and in expediting mutagenesis [3, 4]. The function of DNA hairpins may be correlated to its structure, which fluctuates between two distinct conformations, i.e., (i) zipped (folded) and (ii) unzipped (unfolded). While the zipped state has a low enthalpy because of base pairing, the unzipped state is characterized by a high entropy due to the large number of conformations available to a single DNA chain. The force induced unzipping transition of DNA is different from that of the thermal melting transition [5–7]. In recent years, the zipping/unzipping conformational transition of DNA have been investigated via single molecule micromanipulation experiments [8–10]. The DNA hairpins in such experiments are subjected to a force either via atomic force microscope (AFM) [11–13] or laser tweezers [14, 15] that tends to separate the base pairs at one end of the double helix. The resultant molecular end-to-end extension is measured in terms of appropriate reaction coordinates that parameterizes the free energy profile associated with different conformations of hairpins [1, 16]. The critical value of this applied force estimates the stability of the duplex state relative to the strand separated state. For a critical value of the applied force, the DNA hairpin continuously fluctuates between the folded and unfolded conformations, which may be represented by a double well with two distinct minima of equal energy separated by a barrier. Thus, at equilibrium, the conformational transition of the hairpin between the two equally probable states may be theoretically modeled by a symmetric bistable potential [17–20].

J. Stat. Mech. (2020) 073411

Modern experimental techniques such as Förster resonance energy transfer (FRET) [21–23] and single molecule force spectroscopy (SMFS) [24–28] probe the zipping/unzipping transition of DNA hairpins through transition path time analysis by measuring the equilibrium response of the reaction coordinate [19, 20]. This reaction coordinate may be the distance between the two ends or base pairs of DNA. Transition path times provide microscopic information about the conformational transitions of biomolecules [29–31]. For transitions between the stable/metastable states separated by a barrier, transition paths are a small subset of the stochastic trajectory which just corresponds to the barrier crossing for the first time, without recrossing. Typically, transition times are very small, and the DNA hairpin mostly resides in either of the minima in a bistable potential. Currently, high time resolution experiments are able to measure the average transition path times in nucleic acid and protein folding. Theoretical analysis of transition path times are also developed to obtain transition path time distributions [31–34]. Most of these studies employ Markovian dynamics without memory, while some recent works account for the memory effects in heterogeneous cellular environments, which results in anomalous non-Markovian dynamics of the system [34–39].

This work aims to investigate the stochastic dynamics associated with the conformational transitions of a DNA hairpin in a complex cellular environment within the tenets of Generalized Langevin Equation (GLE). The transition path time distributions for the zipping/unzipping transition across an inverted parabolic barrier are evaluated analytically and compared with Kramers's first passage times. Different features of the transition path time and first passage distributions are discussed as functions of time and barrier height or curvature. The results portray a shorter transition path time for the zipping/unzipping transition as compared to the Kramers's first passage time. Notably, the transition path time depicts a counterintutive trend as it takes less time to cross the transition region with an increase in the height of the potential barrier. Both mean first passage time and the mean transition path time increases with an increase in the complexity of the cellular environment due to the caging effect of the DNA hairpin. Our results for the potential energy landscape, probability density, transition path time distribution and the mean transition path time show a good agreement with those of other theoretical and experimental studies.

2. Theory

The dynamics of zipping/unzipping transitions of the DNA-hairpin may be described in terms of a simple one-dimensional diffusion model [40, 41]. A large number of conformational degrees of freedom associated with biopolymers like DNA or RNA, are the fast variables such as positions and velocities of the individual nucleotides (or monomers) [20, 58]. These variables may be pre-averaged (or integrated out) in an effective free energy landscape to a single degree of freedom or a one-dimensional reaction coordinate, which defines a quasi-static-like approximation [20, 58]. Such low-dimensional projections considerably simplify the complex conformational energy landscape of biomolecules and provides an effective control parameter for monitoring this transition, both theoretically and experimentally. The distance between the two termini or randomly selected

J. Stat. Mech. (2020) 073411

base pairs of DNA may be chosen as the one-dimensional reaction coordinate, 'x', which is measured as the DNA hairpin changes its structure in response to an applied force [17, 42, 43]. Biomolecular dynamics in cellular environments are usually considered in the overdamped limit (i.e. $m/\gamma \to 0$), as the contribution of the frictional part due to the viscoelasticity of the cellular medium dominates the inertial part, such that the inertial term may be neglected [20]. Thus the time evolution of the reaction coordinate, x of the hairpin, either from the zipped state to the transition state or from the zipped state to the unzipped state in the viscoelastic cellular environment, may be described in the framework of the overdamped generalized Langevin equation (GLE) [44–46]

$$m\int_0^t \gamma(t-t')\dot{\mathbf{x}}(t')\,\mathrm{d}t' = -\frac{\mathrm{d}\mathbf{U}(x)}{\mathrm{d}x} + \xi(t) \tag{1}$$

where $\mathbf{x}(t)$ is the time dependent reaction coordinate for the extension of a DNA-hairpin and $\mathbf{U}(x)$ represents the effective potential (or the free energy) for the zipping/unzipping transitions. Here, $\xi(t)$ represents the random thermal force with zero mean $\langle\xi(t)\rangle = 0$. This random force is related to the time dependent friction kernel $\gamma(t)$ via the fluctuation-dissipation theorem as

$$\langle\xi(t)\xi(t')\rangle = k_{\mathrm{B}}Tm\gamma(|t-t'|) \tag{2}$$

where the angular brackets denote statistical averaging over the noise ensemble, k_{B} is the Boltzmann constant and T is the temperature of the environment. The transition of the DNA hairpin in a viscoelastic cellular environment is influenced by the long-time correlated thermal fluctuations which determine the extent of interactions of the DNA in the heterogeneous cellular environment. These fluctuations may be approximated by a history dependent frictional memory kernel, which models the retarded motion of the hairpin in the cellular environment. Such types of noise autocorrelations are typically represented by a power-law as [20, 47, 48]

$$\langle\xi(t)\xi(t')\rangle = \frac{k_{\mathrm{B}}T\eta_\beta(|t-t'|)^{-\beta}}{\Gamma(1-\beta)} \tag{3}$$

where, η_β denotes the fractional friction coefficient, which may be expressed as $\eta_\beta = \eta/\tau_{\mathrm{c}}^{(1-\beta)}$, τ_{c} is the correlation time and Γ is the Gamma function. The scaling exponent β determines the degree of heterogeneity (viscoelasticity) of the cellular medium with $0 < \beta \leqslant 1$, where $\beta = 1$ represents homogeneous surroundings and $\beta = 0$ indicates a completely heterogeneous one. Thus equation (3) may be written as,

$$\langle\xi(t)\xi(0)\rangle = \frac{k_{\mathrm{B}}T\eta_\beta t^{-\beta}}{\Gamma(1-\beta)} \tag{4}$$

The conformational rearrangement of the DNA hairpin between two different states is monitored through the stochastic dynamics of the reaction coordinate in a double well potential [16, 19, 40, 42] that denotes the zipping/unzipping structural transition via an unstable transition state. In single molecule experiments, the DNA molecule held under tension is stretched by a force probe (laser tweezers or atomic force microscope).

J. Stat. Mech. (2020) 073411

The extension of DNA is measured as the structure changes from the zipped to the unzipped state due to the applied force. The free energy profiles are determined from the extension trajectories or the force-extension plots. The free energy of transition for the DNA hairpin [19, 42] (20TS10/T4) is estimated for a critical applied force [61, 62] i.e. at $F_{1/2}$, when the DNA molecule continuously flips between the equally probable zipped and the unzipped conformations in a bistable symmetric potential well [17–20]. The validity of this two-state transition model depends on the hairpin sequence for a critical value of the applied force. The DNA hairpin (20TS10/T4) is selected to reconstruct a symmetric free energy profile along the reaction coordinate at constant force [61, 62]. While the lifetimes of the zipped and the unzipped states of DNA are exactly equal [62], this two-state transition is independent of any change in the external force.

A generalized representation of the free energy landscape of the DNA hairpin may be modeled through a confluent hypergeometric function, given by [49, 50]

$$\mathbf{U}(x) = 2k_{\mathrm{B}}T\,\ln\, y_1(A,x) \tag{5}$$

where,

$$y_1(A,x) = \exp\left(-\frac{k_{\mathrm{S}}}{2k_{\mathrm{B}}T}\frac{x^2}{2}\right){}_1F_1\left(\frac{A}{2}+\frac{1}{4},\frac{1}{2};\frac{k_{\mathrm{S}}}{2k_{\mathrm{B}}T}x^2\right), -1/2 \leqslant A \leqslant 1/2$$

Here, ${}_1F_1(\alpha,\gamma,z)$ is the confluent hypergeometric function [51, 52], which represents a generalized potential with arbitrary well depths. k_{S} is the stiffness parameter [42, 43] or the curvature of the barrier and A is a numerical parameter that defines the shape of the potential well. The potential exhibits one, two or no minima depending on various values of the parameter A, for $-1/2 < A < 0$, equation (5) gives a symmetric bistable potential well separated by a single barrier, for $0 \leqslant A \leqslant 1/2$ is a single-well potential and for $A = -1/2$ it assumes the shape of an inverted parabolic potential. The height of the barrier in the double-well potential is governed by the parameter A. The DNA hairpin may be viewed as a single chain of nucleotides (or monomers) connected by Hookean springs [20, 50, 58, 63, 64]. The effective elasticity generates various conformations of this hairpin which correspond to different energies as depicted in the free energy landscape. The shapes of such potential energy landscapes are characterized by different values of the parameters k_{S} and A, that correspond to the stiffness of the chain and the base-pair interactions of the DNA molecule, respectively. Such a generalized potential (given in equation (5)) may reproduce an entire range of single, double or no-well potential energy surfaces for $-1/2 \leqslant A \leqslant 1/2$, with different barrier heights/curvatures for different values of k_{S}, which may be associated with different types of conformational transitions in DNA hairpins, RNA or proteins or semiflexible polymers in different environments [42, 60]. Figure 1 represents various realizations of the potential $\mathbf{U}(x)$ for different values of A.

Equation (1) may be recast into an effective Fokker–Planck equation (EFPE) (the calculation details are provided in appendix A), which may be expressed as

$$\frac{\partial P(x,t)}{\partial t} = D(t)\left[\frac{\partial^2}{\partial x^2}+\frac{\partial}{\partial x}\frac{\mathbf{U}'(x)}{k_{\mathrm{B}}T}\right]P(x,t) \tag{6}$$

J. Stat. Mech. (2020) 073411

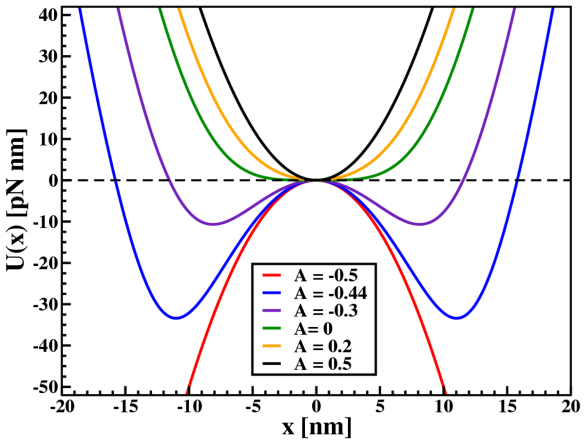

Figure 1. The potential $\mathbf{U}(x)$ as a function of reaction coordinate x (i.e. the molecular extensions) of the DNA hairpin, derived from equation (5). Different shapes of the potential well correspond to different values of parameter A: $A = 0.5$ (black), 0.2 (orange), 0 (green), −0.3 (violet), −0.44 (blue) and −0.5 (red), with $k_{\rm S} = 1$ pN nm^{-1} and $k_{\rm B}T = 10$ kJ mol^{-1} = 16.54 pN nm.

where $P(x, t)$ denotes the time evolution of the probability density of the reaction coordinate x of the DNA hairpin in a symmetric bistable potential well at time t. Here, $\mathbf{U}(x)$ represents the effective potential, the prime indicates the derivative of $\mathbf{U}(x)$ with respect to the reaction coordinate x. The first and the second term depict the contributions of the diffusion and drift-diffusion part, respectively, and $D(t)$ represents the time-dependent diffusion coefficient of the hairpin. The time dependent diffusion coefficient in equation (6) may be expressed as (the details of the calculation are given in appendix A)

$$D(t) = \frac{k_{\rm B}T}{k_{\rm S}} \frac{\dot{\mathcal{Z}}(t)}{\mathcal{Z}(t)} \tag{7}$$

where $\mathcal{Z}(t) = E_{\beta,1}\left(\frac{k_{\rm S}}{\eta_\beta}\, t^\beta\right)$, $E_{a,b}$ denotes the two-parameter Mittag–Leffler function [53]. The expression for $\mathcal{Z}(t)$ may be recast as

$$\mathcal{Z}(t) = E_{\beta,1}\left(D_\beta \frac{k_{\rm S}}{k_{\rm B}T}\, t^\beta \right) \tag{8}$$

Here, $D_\beta = \left(\frac{k_{\rm B}T}{\eta_\beta}\right)$ nm^2 μs$^{-\beta}$ and for $\beta = 1$, $D_1 = \left(\frac{k_{\rm B}T}{\eta}\right)$ nm^2 μs^{-1} where, D_1 represents the normal diffusion coefficient for the transition of the DNA hairpin [19, 42] (20TS10/T4) in a completely homogeneous environment whereas, D_β denotes the diffusion coefficient in heterogeneous environments. The scaling exponent β depicts the degree of heterogeneity/ complexity of the environment with $0 < \beta \leqslant 1$, where $\beta = 1$ corresponds to completely homogeneous surroundings. These two diffusion coefficients may be related as $0 < \frac{D_\beta}{D_1} \leqslant 1$, where the complexity of the surroundings considerably retards the structural dynamics of the DNA hairpin as compared to that in a complete

J. Stat. Mech. (2020) 073411

homogeneous medium. The typical value of the diffusion coefficient of the DNA hairpin [19, 42] (20TS10/T4) in homogeneous environments is estimated as $D_1 = 0.1\,\mathrm{nm}^2\,\mu\mathrm{s}^{-1}$.

2.1. Exact computation of the probability distribution functions

The solution of the effective Fokker–Planck equation [54, 55] (EFPE) in a symmetric bistable potential $\mathbf{U}(x)$ defined by equation (5) may be expressed in terms of the conditional probability distribution function, $P(x, t|x_0)$, which denotes the probability of finding the reaction coordinate, x, at time t, provided the transition trajectory commences at x_0 at time $t = 0$. The modified expression of EFPE may be written as

$$\frac{\partial P(x,t|x_0)}{\partial t} = D(t)\left[\frac{\partial^2}{\partial x^2} + \frac{\partial}{\partial x}\frac{\mathbf{U}'(x)}{k_\mathrm{B}T}\right]P(x,t|x_0) \tag{9}$$

The equation may be solved by the separation of variables (details given in appendix C). The bilinear expansion of $P(x, t|x_0)$ may be simplified as

$$\begin{aligned} P(x,t|x_0) = {} & \frac{P_\mathrm{s}^{1/2}(x)}{P_\mathrm{s}^{1/2}(x_0)}\psi_0(x)\psi_0(x_0) + \sum_{n=0}^{\infty}\frac{P_\mathrm{s}^{1/2}(x)}{P_\mathrm{s}^{1/2}(x_0)}\psi_{n+1}(x)\psi_{n+1}(x_0) \\ & \times \exp\left(-\lambda_{n+1}\int_0^t D(t')\,\mathrm{d}t'\right) \end{aligned} \tag{10}$$

where, $P_\mathrm{s}(x)$ denotes the stationary solution of equation (9), $\psi(x)$ and $\lambda_n(x)$ respectively represent the eigenfunctions and eigenvalues. The detailed solution of the eigenfunctions and eigenvalues of $P(x, t|x_0)$ are provided in appendix C, while the evaluation of the normalization constants C_0 and C_{n+1} are given in appendixes D and E respectively. Substituting the values of the spatial part, $P_\mathrm{s}(x)$, $\psi_0(x)$, $\psi_{n+1}(x)$, C_0 and C_{n+1} from equations (C.3), (C.17), (C.18), (D.5) and (E.6) (derived in the appendixes C, D and E) and the temporal part from equation (C.20) (derived in appendix C) in equation (10), the conditional probability distribution function $P(x, t|x_0)$, may be expressed as

$$\begin{aligned} P(x,t|x_0) = {} & C_0^2\sqrt{\frac{k_\mathrm{S}}{k_\mathrm{B}T}}\frac{1}{(y_1(A,x))^2} + \sum_{n=0}^{\infty}C_{n+1}^2\sqrt{\frac{k_\mathrm{B}T}{k_\mathrm{S}}}(y_1(A,x_0))^2 \\ & \times\frac{\mathrm{d}}{\mathrm{d}x}\frac{D_n(x)}{y_1(A,x)}\frac{\mathrm{d}}{\mathrm{d}x_0}\frac{D_n(x_0)}{y_1(A,x_0)}\mathcal{Z}(t)^{-\left(n+A+\frac{1}{2}\right)} \end{aligned} \tag{11}$$

3. First passage time distribution and mean first passage time

First passage time [44, 56, 57] is defined as the characteristic time required by the DNA hairpin for transition from one conformation to another for the first time, or in other words, it is the time required by the reaction coordinate to traverse from one minima to the other in the free energy landscape for the first time, including the time taken by the DNA to reside in its preferred conformation with recrossings. First passage time is typically referred to as the Kramers's first passage time [31, 66]. Appropriate boundaries

J. Stat. Mech. (2020) 073411

for these transitions must be defined around the potential well to obtain finite passage time distributions.

The dynamics of the DNA hairpin may be viewed as a diffusion in a bistable potential well as established through various single molecule experiments [16, 19, 40, 42]. Since the free energy of the zipped and the unzipped states are almost equal, the DNA molecule can continuously flip between the two states located at potential wells of equal depths [17, 18, 20]. Thus the zipped DNA hairpin (Z) situated at the local minimum of the left potential well (x_A), may either reach (i) a transition state at the top of the barrier (x_B as $x_B = 0$) i.e., 'zipped to transition state' ($Z \rightarrow Z_{\rm TS}$) or (ii) the unzipped state of comparable energy at the right potential well ($x_{\rm C}$) via 'zipped to unzipped state' transition ($Z \rightarrow Z_{\rm U}$). Each of these transitions are defined in terms of the diffusion of the respective reaction coordinate in the transition trajectory with appropriate boundary conditions. The zipped state of the DNA hairpin may be considered as a reflecting boundary for the transitions induced by the external force till it acquires either the transition state or the unzipped state, via (i) and (ii). While, the transition state is considered as an absorbing boundary for (i), the unzipped state is represented as the absorbing boundary for (ii). The transitions (i) and (ii) are regarded as decoupled. The first passage time distribution (FPTD) for each of these transitions may be evaluated from their respective conditional probability distribution profiles as [56, 67, 73] (derived in appendix F)

$$\mathcal{F}(x_0,t) = -\frac{\mathrm{d}}{\mathrm{d}t}\int_{x_A}^{x_B/x_C} P(x,t|x_0)\,\mathrm{d}x \tag{12}$$

where, the limits of the definite integral correspond to different conformations during the transitions (i) and (ii) and Z, $Z_{\rm U}$ and $Z_{\rm TS}$ denote the zipped, unzipped and the transition (intermediate) states of the DNA hairpin with the reaction coordinates x_A, x_C and x_B respectively. The first passage time distribution, $\mathcal{F}(x_0,t)$ of either transitions (i) or (ii) for any arbitrary position x_0, located in the interval $x_A < x_0 < x_B = 0$ for (i) and $x_A < x_0 < x_B = 0 < x_C$ for (ii) in complex cellular environments, may be represented as

$$\begin{aligned}\mathcal{F}(x_0,t) = \sum_{n=0}^{\infty} C_{n+1}^2 \sqrt{\frac{k_{\rm B}T}{k_{\rm S}}}\left(y_1(A,x_0)\right)^2 \frac{\mathrm{d}}{\mathrm{d}x_0}\frac{D_n(x_0)}{y_1(A,x_0)}\left[\frac{D_n(x)}{y_1(A,x)}\right]\Bigg|_{x_A}^{x_B/x_C}\left(D_\beta \frac{k_{\rm S}}{k_{\rm B}T}\,t^{\beta-1}\right)\\ \times\left(n+A+\frac{1}{2}\right)E_{\beta,\beta}\left(D_\beta\frac{k_{\rm S}}{k_{\rm B}T}\,t^{\beta}\right)\left(E_{\beta,1}\left(D_\beta\frac{k_{\rm S}}{k_{\rm B}T}\,t^{\beta}\right)\right)^{-(n+A+\frac{3}{2})}\end{aligned} \tag{13}$$

The mean first passage time [67], $\bar{\tau}$, is a measure of the average time required for either conformational transitions (i) or (ii) such that the transition trajectory may recross and revisit the initial conformation until it reaches the final state. Mathematically, the first moment of the first passage time distribution over the entire period of observation defines the mean first passage time as, $\bar{\tau} = \int_0^\infty t\mathcal{F}(x_0,t)\mathrm{d}t$. Thus, the MFPT of the conformational transitions (i) and (ii) of the DNA hairpin subject to the memory

J. Stat. Mech. (2020) 073411

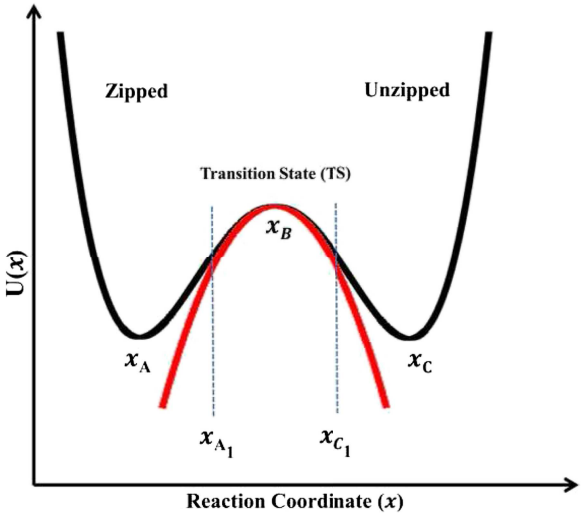

Figure 2. Schematic representation of the conformational transition of the hairpin typically modeled as a diffusive dynamics of the reaction coordinate x in a symmetric bistable potential. The hairpin continuously flips between the zipped (x_A) and the unzipped (x_C) state located at the potential minima via a transition state at the barrier top (x_B). Transition paths are the parts of the entire molecular trajectory (i.e. from $x_A < x < x_C$) that is confined within $x_{A_1} < x < x_{C_1}$, when the trajectory starts at x_{A_1} and exits at x_{C_1}.

effects due to the complex (viscoelastic) cellular environments, may be evaluated as

$$\bar{\tau} = \sum_{n=0}^{\infty} C_{n+1}^2 \sqrt{\frac{k_{\rm B}T}{k_{\rm S}}} (y_1(A, x_0))^2 \frac{\rm d}{{\rm d}x_0} \frac{D_n(x_0)}{y_1(A, x_0)} \left[\frac{D_n(x)}{y_1(A, x)}\right]\Bigg|_{x_A}^{x_B/x_C} \times \left(\frac{k_{\rm B}T}{k_{\rm S}D_\beta}\right)^{1/\beta} \left(\frac{2\,\Gamma(1+\beta)}{(2n+2A+1)}\right) \tag{14}$$

4. Transition path time distribution

Transition path time (TPT) may be defined as the time required by the DNA hairpin to just cross the potential barrier i.e., the trajectory of the reaction coordinate from x_{A_1} (or x_{C_1}) located at one side of the potential barrier to x_{C_1} (or x_{A_1}) at the other side of the barrier, without recrossing x_{A_1} (or x_{C_1}). Figure 2 is a schematic representation of a part of the trajectory that commences at x_{A_1} and terminates at x_{C_1}, without revisiting the initial position x_{A_1} or viceversa. The transition path time distribution in the confined domain $x_{A_1} < x_B < x_{C_1}$ may be obtained from the relevant boundary conditions. For the zipping/unzipping transition, absorbing boundary conditions at x_{A_1} and x_{C_1} of the trajectory correspond to the vanishing probability of the hairpin at these positions and thus defines a complete two-state transition. The absorbing boundary at x_{A_1} and x_{C_1} also prohibits recrossing of the trajectory to revisit the initial state. This two-state transition in a bistable symmetric potential obtained from the generalized expression of $\mathbf{U}(x)$ in equation (1) for the value of $A = -1/2$, may be expressed as

J. Stat. Mech. (2020) 073411

$$\mathbf{U}(x)|_{A=-\frac{1}{2}} = 2k_{\mathrm{B}}T\,\ln\left[\,\exp\left(-\frac{k_{\mathrm{S}}}{2k_{\mathrm{B}}T}\frac{x^2}{2}\right)\right] = -\frac{k_{\mathrm{S}}\,x^2}{2} \tag{15}$$

Therefore, the transition path time distribution (TPTD), $\mathcal{P}_{\mathrm{TPT}}(t)$ for the DNA hairpin to dwell in the confined region $x_{A_1} < x < x_{C_1}$, defined by the potential in equation (15), before it is absorbed at either x_{A_1} or x_{C_1}, satisfies the equation

$$\mathcal{P}_{\mathrm{TPT}}(t) = -\frac{\mathrm{d}}{\mathrm{d}t}\int_{x_{A_1}}^{x_{C_1}} P(x,t|x_0)|_{A=-\frac{1}{2}}\,\mathrm{d}x \tag{16}$$

where, the probability distribution $P(x,t|x_0)$ of the reaction coordinate may be obtained as a special case with $A=-\frac{1}{2}$ from the equation (11). The mean transition path time [33, 66, 68], $\bar{\tau}_{\mathrm{TPT}}$ may be defined as the average time required for a transition between two conformations located at either sides of the potential barrier between x_{A_1} and x_{C_1}. Analytically, it is the first moment of TPT distribution of the DNA hairpin along the transition path, which may be expressed as $\bar{\tau}_{\mathrm{TPT}} = \int_0^\infty t\mathcal{P}_{\mathrm{TPT}}(t)|_{A=-1/2}\mathrm{d}t$.

The mean transition path time (MTPT) of the DNA hairpin may be obtained from equation (11) with $A=-\frac{1}{2}$, which is expressed as

$$\bar{\tau}_{\mathrm{TPT}} = \sum_{n=1}^{\infty}\frac{2^{-n}}{\sqrt{\pi}}\frac{\Gamma(1+\beta)}{nn!}\left(\frac{k_{\mathrm{B}}T}{k_{\mathrm{S}}D_\beta}\right)^{1/\beta}\exp\left(-\frac{k_{\mathrm{S}}\,x_0^2}{2k_{\mathrm{B}}T}\right)H_{n-1}\left(\sqrt{\frac{k_{\mathrm{S}}}{2k_{\mathrm{B}}T}}x_0\right) \times H_n\left(\sqrt{\frac{k_{\mathrm{S}}}{2k_{\mathrm{B}}T}}x\right)\Bigg|_{x_{A_1}}^{x_{C_1}} \tag{17}$$

where, $n \geqslant 1$ represents the non trivial solution of the equation and $H_n(x)$ denotes the Hermite polynomials [51, 71]. Equation may also be written in the terms of the barrier height, ΔE as

$$\bar{\tau}_{\mathrm{TPT}} = \sum_{n=1}^{\infty}\frac{2^{-n}}{\sqrt{\pi}}\frac{\Gamma(1+\beta)}{nn!}\left(\frac{k_{\mathrm{B}}T}{k_{\mathrm{S}}D_\beta}\right)^{1/\beta}\exp\left(-\frac{\Delta E}{k_{\mathrm{B}}T}\right)H_{n-1}\left(\sqrt{\frac{\Delta E}{k_{\mathrm{B}}T}}\right) \times H_n\left(\sqrt{\frac{k_{\mathrm{S}}}{2k_{\mathrm{B}}T}}x\right)\Bigg|_{x_{A_1}}^{x_{C_1}} \tag{18}$$

where,

$$\frac{\Delta E}{k_{\mathrm{B}}T} = \frac{k_{\mathrm{S}}\,x_0^2}{2k_{\mathrm{B}}T} \tag{19}$$

denotes the relation between the dimensionless barrier height of the potential (also, known as barrier energy) with curvature of the potential barrier. Figure 3 presents a schematic representation of the zipping/unzipping transitions of a DNA hairpin for the potential defined by equation (15), with different curvatures k_{S} of the potential barrier for a particular x_0. Three different curvatures portray different heights of the potential barrier, that are linearly related to each other by equation (19), such that increasing

J. Stat. Mech. (2020) 073411

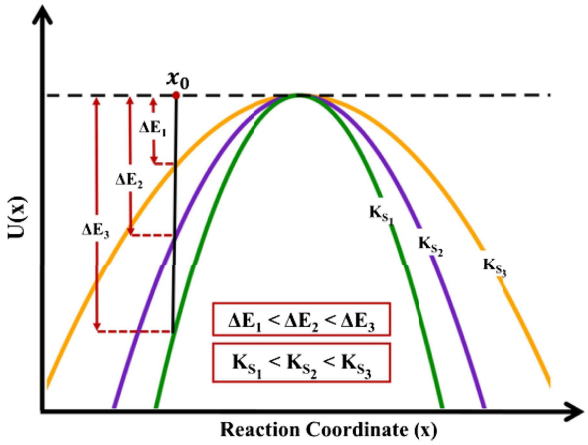

Figure 3. Schematic representation of the transition paths for the zipping/unzipping transition of a DNA hairpin as a function of reaction coordinate x, with different barrier heights for a fixed x_0. The increase in curvature k_S of the potential barrier; $k_{S_1} < k_{S_2} < k_{S_3}$ may be related to the corresponding barrier heights (or barrier energy) as $\Delta E_1 < \Delta E_2 < \Delta E_3$.

order of curvature $k_{S_1} < k_{S_2} < k_{S_3}$ corresponds to an increase in the barrier heights as $\Delta E_1 < \Delta E_2 < \Delta E_3$ with a consequent increase in the barrier energy.

5. Results and discussion

The bistable symmetric free energy landscape obtained from equation (5), is matched with the experimentally determined potential for the zipping/unzipping transition of the DNA hairpin [16, 19, 40, 42] for $A = -0.44$, $\beta = 1$ and $k_S = 1\,\mathrm{pN\,nm^{-1}}$. Equation (5) represents the generalized symmetric bistable potential with arbitrary well depths. The corresponding probability distribution function, $P(x, t|x_0)$, obtained from equation (11) represents the experimental distribution function, which is depicted as a function of the molecular extension of the hairpin, x. A comparison of the experimental and theoretical studies reveal an excellent agreement between the energy landscape obtained from equation (5) with that reconstructed from the single molecule force spectroscopy measurements, without the deconvolution of the instrumental effects [42, 65]. The key feature of such reconstructions from the single molecule trajectories include the effects of tether compliance that complicates the estimation of the real energy profiles of the molecule, thus making the deconvolution [16, 17, 42, 65] mandatory. This theoretical method captures the essential features like the exact height and the position of the both energy and probability profiles of the DNA hairpin as compared to those extracted from the deconvoluted SMFS experimental data.

Figure 4 compares the results for the zipping/unzipping transitions of the DNA hairpin (20TS10/T4) obtained from our theory with those of the single molecule experiments of Woodside *et al* [42]. Figure 4(a) and (b) represent the potential energy landscape of the DNA hairpin and its corresponding probability density function, respectively. The results calculated from our theory (from equation (5) and equation (11)) for $A = -0.44$,

J. Stat. Mech. (2020) 073411

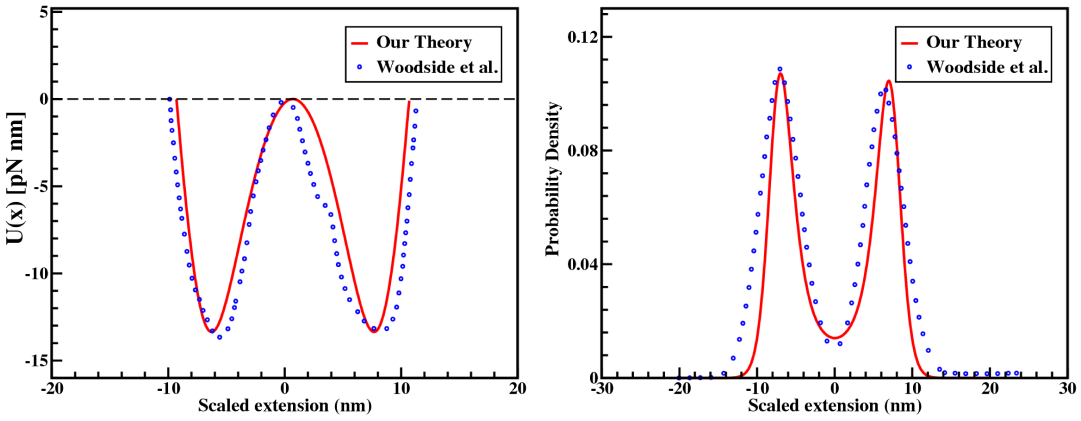

(a) (b)

Figure 4. Comparison plots (a) and (b) show the potential energy landscape and the probability density function for the zipping/unzipping transition of the DNA hairpin (20TS10/T4), respectively. Results obtained from our theory (in red) are compared with those obtained from the single molecule experiments of Woodside *et al* [42].

$k_S = 1\,\mathrm{pN\,nm^{-1}}$ at time $t = 7000\,\mu\mathrm{s}$, show a good agreement with those obtained from the single molecule experiments of DNA hairpin by Woodside *et al* [42].

Figure 5 shows the first passage time distribution function (FPTD), $\mathcal{F}(t)$, for the conformational transition of the DNA hairpin (derived from equation (13)) plotted as a function of time t, for three different values of β and D_β as $D_{0.8} = 0.08\,\mathrm{nm^2\,\mu s^{-(0.8)}}$, $D_{0.9} = 0.09\,\mathrm{nm^2\,\mu s^{-(0.9)}}$ and $D_1 = 0.1\,\mathrm{nm^2\,\mu s^{-1}}$ for $\beta = 0.8$ (blue), $\beta = 0.9$ (red) and $\beta = 1$ (black), respectively for two different barrier heights corresponding to $A = -0.34$ and $A = -0.44$.

Different values of the parameter A are used to depict different barrier heights (i.e. from the bottom of the well to the barrier top) of the symmetric double well potential. The value $A = -0.44$ is extracted from an exact match with the experimentally fitted data [42]. The value $A = -0.34$ is arbitrarily chosen to portray the effect of any change in the system compliance [42], which is evident from the reconstruction of a similar bistable symmetric potential of DNA, with a different barrier height as compared to that obtained for $A = -0.44$.

Figure 5(a) and (b) illustrate the FPTD of transition of the zipped DNA hairpin via (i) and (ii), respectively. These distributions are obtained by truncating the infinite series of $\mathcal{F}(t)$ (refer to equation (13)) and retaining up to 1000 terms. This truncation retains the accuracy of the results even for higher order terms. FPTD for both transitions is represented by a unimodal peak of an asymmetric distribution for each value of β with different barrier heights. The amplitudes of the peaks decrease with a decrease in the values of β for each transition.

Smaller values of β implies that the complexity of the surroundings increases with an increase in the correlations between thermal fluctuations. Thus, it retards the dynamics of the zipped DNA which results in lower FPTD for either transitions. The higher β values corresponds to a surroundings with a lower complexity, that results in faster

J. Stat. Mech. (2020) 073411

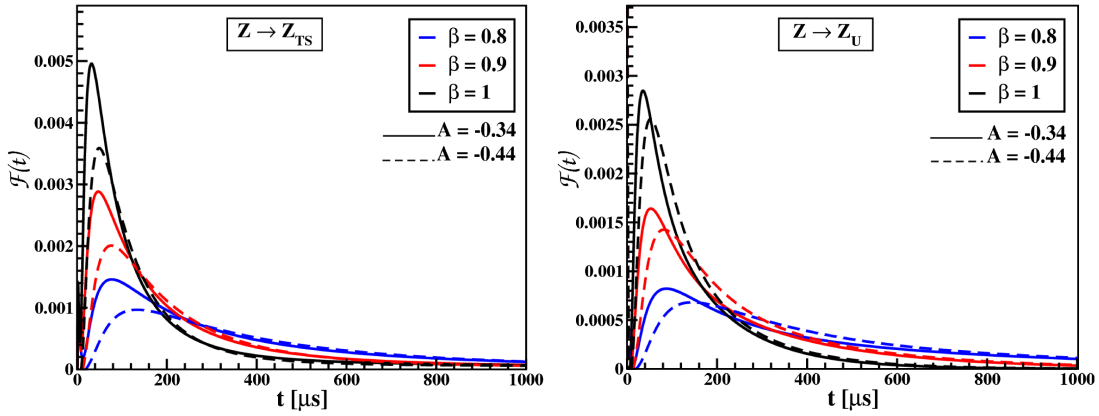

(a) Transition (i) (b) Transition (ii)

Figure 5. The first passage time, $\mathcal{F}(t)$ versus time for the conformational transitions of DNA hairpin in a double well potential as obtained from equation (13) for varied barrier heights represented by parameter $A = -0.34$ and $A = -0.44$, respectively. The solid and dashed lines in the plot correspond to $D_{0.8} = 0.08\,\mathrm{nm}^2\,\mu\mathrm{s}^{-(0.8)}$, $D_{0.9} = 0.09\,\mathrm{nm}^2\,\mu\mathrm{s}^{-(0.9)}$ and $D_1 = 0.1\,\mathrm{nm}^2\,\mu\mathrm{s}^{-1}$ for $\beta = 0.8$ (blue), $\beta = 0.9$ (red) and $\beta = 1$ (black), respectively. Plots (a) and (b) represent the respective transitions (i) and (ii).

structural motions of DNA hairpin, with lower FPT. A comparison of the FPTD for two different barrier heights in the potential well for $A = -0.34$ and $A = -0.44$, is portrayed for each of the transition events. The FPTD increases with a decrease in the barrier height of the potential well. The amount of energy required to reach the barrier top increases with an increase in the height of the potential barrier, which reduces the probability of transition via either routes (i) or (ii). Hence both transitions require longer times as reflected in broader distributions of the FPT with lower amplitudes. The probability distribution profile of the first passage times for two different transitions obtained from figure 5 exhibits that the transition of the zipped DNA hairpin to the transition state at the barrier top is more probable as compared to that of the unzipped state located at the bottom of another potential well. The zipping/unzipping transition requires more energy to reach the unzipped state and hence there is a lower probability for the unzipped state.

Figure 6 represents the MFPT $\bar{\tau}$ of the conformational transitions of the DNA hairpin for both transitions as a function of the reaction coordinate x_0 as derived from equation (14). Figure 6(a), presents the MFPT of DNA for three different β values; $\beta = 0.8$(blue), $\beta = 0.9$(red) and $\beta = 1$(black) with $A = -0.44$ and $k_S = 1\,\mathrm{pN\,nm}^{-1}$. The dashed lines in the plot represents transition (i) of the DNA hairpin, whereas solid lines denote (ii). MFPT for both transitions exhibit a monotonic increase with a decrease in the β value, which then becomes constant. The mean time for both transitions records a minimum value when they originate close to the zipped or unzipped state located at either potential minimum. As x_0 increases for both transitions (i) and (ii), the corresponding time required also increases as the hairpin reaches or crosses the potential barrier starting from either states [67].

J. Stat. Mech. (2020) 073411

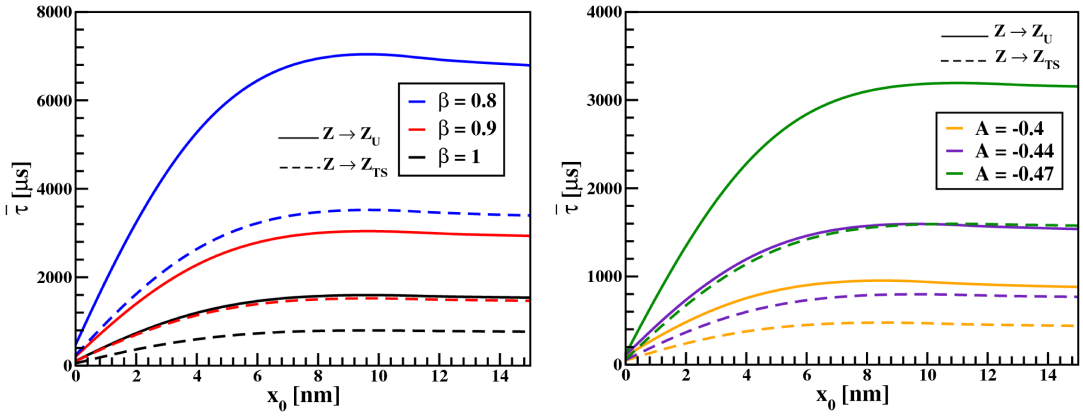

Figure 6. The mean first passage time $\bar{\tau}$ versus the initial reaction coordinate of the trajectory of the DNA hairpin derived from equation (14). Plot (a) corresponds to the MFPT with different values of β; $\beta = 0.8$ (blue), $\beta = 0.9$ (red) and $\beta = 1$ (black), with $A = -0.44$ and $k_S = 1$ pN nm^{-1}. Plot (b) depicts the MFPT of DNA hairpin for different barrier heights denoted by parameter A; $A = -0.4$, $A = -0.44$ and $A = -0.47$, with $\beta = 1$ and $k_S = 1$ pN nm^{-1}. The dashed lines denote the transitions (i) while solid lines denote (ii).

However, the results indicate that the MFPT for transition (ii) is higher than that for (i). Since, transition (ii) comprises a longer trajectory as compared to (i), therefore the MFPT for (ii) is higher than that of (i). MFPT for both the transitions is shown in figure 6(b), for three different barrier heights, denoted by the parameter A; $A = -0.4$, $A = -0.44$ and $A = -0.47$, with $\beta = 1$ and $k_S = 1$ pN nm^{-1}. MFPT of the DNA hairpin increases with the increase in the barrier height of the potential well, for both transitions (i) and (ii). For both transitions, the zipped DNA covers a longer trajectory with an increase in the heights of the potential barrier which results in longer MFPTs.

Figure 7 represents the transition path time distribution, $\mathcal{P}_{\rm TPT}(t)$ derived from equation (16) for the zipping/unzipping transitions of the DNA hairpin as a function of time. Figure 7(a) depicts the TPTD of DNA for three different values of β with D_β as $D_{0.8} = 0.08\,\mathrm{nm}^2\,\mu\mathrm{s}^{-(0.8)}$, $D_{0.9} = 0.09\,\mathrm{nm}^2\,\mu\mathrm{s}^{-(0.9)}$ and $D_1 = 0.1\,\mathrm{nm}^2\,\mu\mathrm{s}^{-1}$ for $\beta = 0.8$ (blue), $\beta = 0.9$ (red) and $\beta = 1$ (black), respectively, with $k_S = 1\,\mathrm{pN\,nm}^{-1}$ and $x_0 = -1$ nm. The distributions displayed in the plot are obtained by truncating the infinite series of $\mathcal{P}_{\rm TPT}(t)$ (refer to equation (16)) and retaining up to 1000 terms. This truncation is sufficient enough to ensure that the results are accurate. The results reveal that the amplitudes of the TPT distribution peaks decrease with a decrease in the value of β. For higher complexity/heterogeneity of the surroundings (lower the value of β) due to increased correlations between thermal fluctuations, the TPT of the DNA hairpin is higher for the zipped/unzipped transition. The complex viscoelastic environment impede the structural motions of the DNA due to the 'caging' effect [69], which restricts its conformational transitions resulting in higher transition path times.

A comparison of the figures 7(a) and 5(b) demonstrates that the TPT for the structural transition of the DNA hairpin is smaller than its corresponding first passage time.

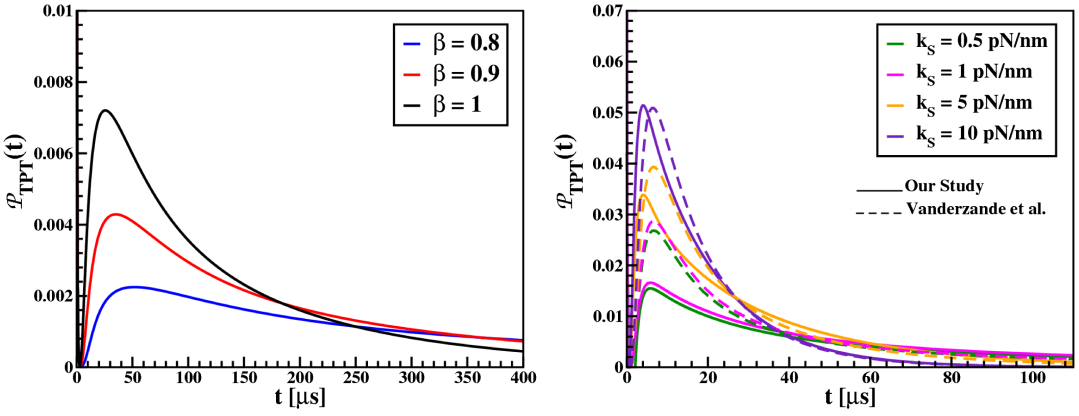

Figure 7. The transition path time distribution, $\mathcal{P}_{\rm TPT}(t)$ versus time, for the zipping/unzipping transitions as obtained from equation (16) with $A = -\frac{1}{2}$. Plot (a) shows the TPTD of DNA for three different β values as; $\beta = 0.8$ (blue), $\beta = 0.9$ (red) and $\beta = 1$ (black) with $k_{\rm S} = 1$ pN nm^{-1}. Plot (b) represents a comparative plot of the TPTD calculated from our theory with that estimated from Vanderzande *et al* [34], for different values of barrier curvature $k_{\rm S}$; with $k_{\rm S} = 0.5$ pN nm^{-1} (green), $k_{\rm S} = 1$ pN nm^{-1} (magenta), $k_{\rm S} = 5$ pN nm^{-1} (orange) and $k_{\rm S} = 10$ pN nm^{-1} (violet).

This is due to the fact that the TPT estimates the time required to just cross the barrier and comprises a small subset of the entire trajectory. However, FPT evaluates the total time for the conformational transition, which is the sum of the TPT and the residence time of the DNA hairpin to be in its preferred conformation at the potential minimum. Figure 7(b), represents the $\mathcal{P}_{\rm TPT}(t)$ of the DNA hairpin for the transition in a potential barrier of different heights, for different values of the curvature of the potential barrier (or stiffness parameter), $k_{\rm S}$; with $k_{\rm S} = 0.5$ pN nm^{-1}, $k_{\rm S} = 1$ pN nm^{-1}, $k_{\rm S} = 5$ pN nm^{-1} and $k_{\rm S} = 10$ pN nm^{-1} with $\beta = 1$. Since, $\frac{\Delta E}{k_{\rm B}T} = \frac{k_{\rm S}\ x_0^2}{2k_{\rm B}T}$ (from equation (19)), therefore a change in the value of k_S for a constant x_0 or vice versa (i.e. change in x_0 with constant k_S) determines the change in the height/curvature of the inverted parabolic potential as shown in figure 3. The results obtained exhibit a counterintuitive trend, which indicate that the transition path time decreases with an increase in the barrier height, for a fixed length of the barrier region [32, 33, 59, 66, 68]. Figures 2 and 3, show that the transition paths between the confined domain x_{A_1} and x_{C_1} vary with barrier heights, which corresponds to a change in values of the curvature, k_S. Thus higher the barrier (i.e. with higher k_S), the sharper is the curvature of the barrier in the transition region of fixed length, which implies that less time is required for the transitions across a higher barrier with a sharper curvature as compared to those with lower barrier heights and broader curvature. This means that a lesser distance is traversed to cross a barrier with a sharper curvature as compared to that of a broader one. Thus the TPTs are lower for a higher barrier as compared to those for a lower one with a broader curvature. Therefore, TPTs decrease with an increase in the barrier height [32, 33, 59, 66, 68].

J. Stat. Mech. (2020) 073411

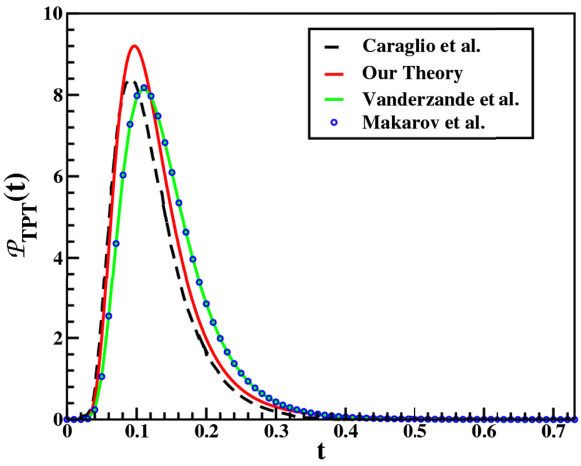

Figure 8. A comparison of $\mathcal{P}_{\rm TPT}(t)$ obtained from our theory (equation (16)), denoted by red solid line, with that of Caraglio *et al* [32] approach (in black dashed line), for the absorbing boundary conditions. A comparison of the TPTDs obtained for the free boundary conditions by Vanderzande [34] (in green solid line) and Makarov *et al* [33] (in blue circles) with that of our theory for the absorbing boundary conditions with arbitrary parameters $k_S = 8$, $x_0 = 1$ and $\beta = 1$.

However, TPTs increase with an increase in the length of the barrier region between two absorbing boundaries, for a fixed k_S (or barrier curvature). The energy of the system is conserved for the zipping/unzipping transition. The hairpin draws thermal energy from the environment for this conformational transition across the barrier. Therefore, higher the potential barrier, greater is the energy required to surmount the barrier. According to the principle of conservation of energy, the greater the thermal energy the zipped DNA extracts from the surroundings to climb the barrier top, the faster it crosses the energy barrier to reach the unzipped state, releasing an equivalent amount of thermal energy in the environment.

Therefore, unlike Kramers's FPT, TPTs decrease with increase in barrier heights. A comparison of the TPT distribution obtained from our theory (denoted by solid lines) for absorbing boundary conditions with that obtained by Vanderzande *et al* [34] (denoted by dashed lines) for the free boundary conditions, reveals that both TPT distributions for different boundary conditions coincide with each other with increasing height of the potential barrier [31, 32].

Figure 8 compares $\mathcal{P}_{\rm TPT}(t)$ for the absorbing boundary conditions from our approach (refer to equation (16)) with the analytical results of Caraglio *et al* [32] for absorbing boundary conditions, Vanderzande *et al* [34] and Makarov *et al* [33, 43] for free boundary conditions with an arbitrary choice of parameters $k_S = 8$, $x_0 = 1$ and $\beta = 1$. The plot reveals that TPT distributions calculated from our theory (in red solid line) is in good qualitative agreement with the analytical results of Caraglio *et al* [32] (in black dashed line) for the absorbing boundary conditions. However the results of TPTD for the free boundary conditions exhibit a relatively broader distribution with a long time tail as compared to the narrower TPT distributions for the absorbing boundary conditions observed at shorter times. The confinement of the transition paths between absorbing

J. Stat. Mech. (2020) 073411

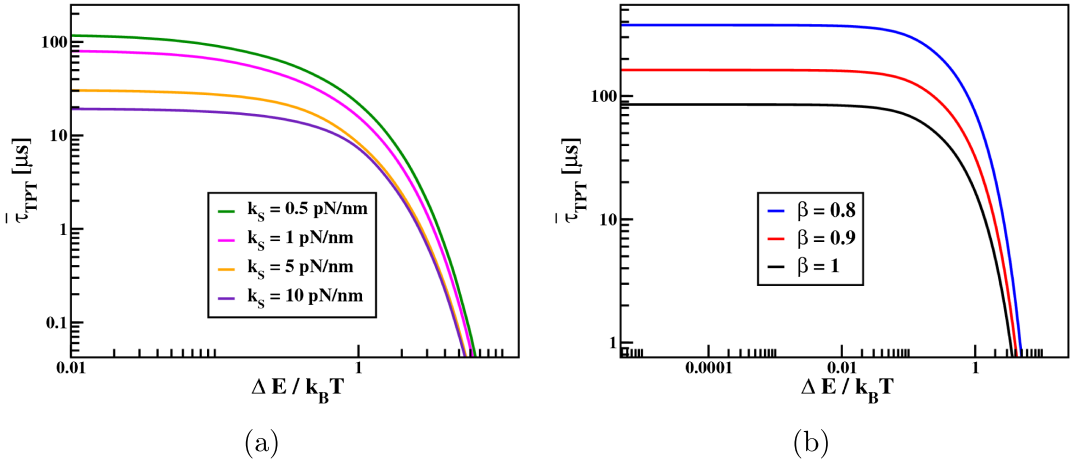

Figure 9. The mean transition path time, $\bar{\tau}_{\rm TPT}$ of the hairpin versus barrier height $\Delta E/k_{\rm B}T$, derived from equation (18). Plot (a) and (b) represent the mean transition time path time (on a log–log scale) for varied k_S values; as $k_S = 0.5$ pN nm^{-1}, $k_S = 1$ pN nm^{-1}, $k_S = 5$ pN nm^{-1}, and $k_S = 10$ pN nm^{-1} and β with $\beta = 0.8$, $\beta = 0.9$, and $\beta = 1$, respectively.

Table 1. A comparison of the mean transition path time for the zipping/unzipping transitions of the DNA hairpin obtained from our theory with that of experiments by Woodside *et al* [19]

Mean transition path time	Our theory	Experiments [19]
DNA hairpin (20TS10/T4)	19.25 μs	16 μs

boundaries results in a narrower distribution of the TPTDs as compared to broader distribution curves for the free boundary condition.

Figure 9 presents the MTPT, $\bar{\tau}_{\rm TPT}$ of the zipping/unzipping transition of the DNA hairpin as a function of the barrier height, $\Delta E/k_{\rm B}T$ (scaled with respect to energy $k_{\rm B}T$), obtained from equation (18). Figures 9(a) and (b) depict the log–log plots of MTPT of DNA for varied barrier curvatures, denoted by different values of the stiffness parameters, k_S as $k_S = 0.5\,{\rm pN\,nm^{-1}}$, $k_S = 1\,{\rm pN\,nm^{-1}}$, $k_S = 5\,{\rm pN\,nm^{-1}}$ and $k_S = 10\,{\rm pN\,nm^{-1}}$ in heterogeneous environments with varying complexity as $\beta = 0.8$, $\beta = 0.9$, and $\beta = 1$, respectively. The MTPT for both the plots shows a monotonic decrease with the increase in the barrier height. Figure 9(a) represents a decrease in MTPT with an increase in k_S, where a subsequent increase in k_S values corresponds to an increase in the barrier height, $\Delta E/k_{\rm B}T$. The TPTD calculations of the DNA hairpin clearly indicate that there is practically no difference between the results obtained for the free and the absorbing boundary conditions for high barrier heights [31]. A comparison of the values of the MTPT of the DNA hairpin(20TS10/T4) obtained from our theory with those obtained from single molecule experiments [19] are shown in table 1.

J. Stat. Mech. (2020) 073411

Table 1 shows a good agreement between the MTPT calculated from this theory and those obtained from the experiments thus proving the validity of the model. This approach may be used independently to evaluate the transition path time for the structural transitions of the DNA hairpin from the exact deconvolved energy landscape constructed from the generalized mathematical equations, thus unraveling the intrinsic dynamics of the molecule. This method is more accurate as compared to the single molecule force experiments, whose data may vary due to the modulation of the experimental artifacts [16, 17, 42, 65]. Figure 9(b), represents the MTPT of the DNA hairpin for a fixed barrier curvature with varying degrees of thermal fluctuations as reflected in different β values as $\beta = 0.8$, $\beta = 0.9$ and $\beta = 1$, as a function of the barrier height. The results predict that the MTPT increases with the increase in the complexity of the surrounding (i.e. decrease in β value), which hinders the structural motions of DNA hairpin and reduces the probability of zipping/unzipping transitions.

6. Conclusions

This work explores the zipping/unzipping transitions of a DNA hairpin in complex cellular environments. Such conformational transitions may be theoretically modeled as the stochastic dynamics of a DNA hairpin in a symmetric double well potential. The results portray that the TPTs for such transitions are lower compared to the Kramers's first passage times. First passage times increase with an increase in barrier heights, whereas TPTs show a counterintuitive trend. Both mean TPT and MFPT increases with an increase in complexity/heterogeneity of the cellular environment due to the 'caging' effect exerted by the surroundings, which retards the motion of the DNA hairpin. The results show a good agreement with other theoretical studies and with the experimentally measured potential energy landscape, probability distribution function and the transition path time distribution of the DNA hairpin. Experimentally measured value of the mean transition path time of the hairpin agrees well with that calculated from theory for high barrier heights.

Acknowledgments

The authors gratefully acknowledge DST-SERB, India (Project No. EMR/2016/006 619), and DU-DST Purse Grant Phase-II (CD/2018/1638) for financial assistance. S Sharma acknowledges University Grant Commission, India for providing financial support in form of a Senior Research Fellowship.

Appendix A. Solution of GLE under symmetric potential

The symmetric potential in equation (5) may be simplified as,

$$\mathbf{U}(x) = -\frac{k_{\mathrm{S}}}{2}x^2 + 2k_{\mathrm{B}}T\ \ln\left[{}_1F_1\left(\frac{A}{2}+\frac{1}{4},\frac{1}{2};\frac{k_{\mathrm{S}}}{2k_{\mathrm{B}}T}x^2\right)\right] \tag{A.1}$$

J. Stat. Mech. (2020) 073411

Substituting the differentiation of equations (A.1) in equation (1), we get

$$-k_{\rm S}\ x(t) + W(x(t)) = -m\int_0^t \gamma(t-t')\dot{x}(t')\,{\rm d}t' + \xi(t). \tag{A.2}$$

where $W(x) = \frac{\rm d}{{\rm d}x}\ 2k_{\rm B}T\ \ln\left[{}_1F_1\left(\frac{A}{2}+\frac{1}{4},\frac{1}{2};\frac{k_S}{2k_{\rm B}T}x^2\right)\right]$

This equation may be solved by Laplace transform, which may be simplified as

$$\tilde{x}(s) = \frac{m\ x_0\tilde{\gamma}(s)}{ms\tilde{\gamma}(s)-k_{\rm S}} + \frac{\tilde{\xi}(s)}{ms\tilde{\gamma}(s)-k_{\rm S}} - \frac{W(\tilde{x}(s))}{ms\tilde{\gamma}(s)-k_{\rm S}}, \tag{A.3}$$

where the Laplace transform of any function is given as $\tilde{f}(s) \equiv \mathcal{L}[f(t)]$. Function $\tilde{\mathcal{Z}}(s)$ may be defined as

$$\tilde{\mathcal{Z}}(s) = \frac{m\ \tilde{\gamma}(s)}{ms\tilde{\gamma}(s)-k_{\rm S}}. \tag{A.4}$$

Substituting the above relation, the inverse Laplace transform of equation (A.3) may be obtained as

$$x(t) = x_0\mathcal{Z}(t) - \frac{1}{k_{\rm S}}\int_0^t \phi(t-t')\xi(t')\,{\rm d}t' + \frac{1}{k_{\rm S}}\int_0^t \phi(t-t')W(x(t'))\,{\rm d}t', \tag{A.5}$$

where the function $\phi(t)$ is the inverse Laplace transform of $\tilde{\phi}(s)$, which is defined by

$$\tilde{\phi}(s) = -\frac{k_{\rm S}}{ms\tilde{\gamma}(s)-k_{\rm S}}. \tag{A.6}$$

The function $\dot{x}(t)$ is obtained from the differentiation of equation (A.5) with respect to t,

$$\begin{aligned}\frac{{\rm d}x(t)}{{\rm d}t} = &-\Upsilon(t)x(t) - \frac{1}{k_{\rm S}}\mathcal{Z}(t)\frac{\rm d}{{\rm d}t}\frac{1}{\mathcal{Z}(t)}\int_0^t \phi(t-t')\xi(t')\,{\rm d}t' \\ &+\frac{1}{k_{\rm S}}\mathcal{Z}(t)\frac{\rm d}{{\rm d}t}\frac{1}{\mathcal{Z}(t)}\int_0^t \phi(t-t')W(x(t'))\,{\rm d}t',\end{aligned} \tag{A.7}$$

where $\Upsilon(t) = -\frac{\dot{\mathcal{Z}}(t)}{\mathcal{Z}(t)}$, and the expression for $\mathcal{Z}(t)$ may be obtained from equation (A.4). The Laplace transform of the memory kernel $\tilde{\gamma}(s)$, for the power-law correlated noise in equation (4) may be calculated via fluctuation-dissipation relation from equation (2), as

$$\tilde{\gamma}(s) = \frac{\eta_\beta}{m}\ s^{\beta-1}. \tag{A.8}$$

From the inverse Laplace transform of the resultant equation obtained by the substitution of the above relation in equation (A.4), we have

$$\mathcal{Z}(t) = E_{\beta,1}\left(\frac{k_{\rm S}}{\eta_\beta}t^\beta\right). \tag{A.9}$$

where $E_{a,b}$ represents the two-parameter Mittag–Leffler function [53].

J. Stat. Mech. (2020) 073411

Appendix B. Transformation of GLE to effective Fokker–Planck equation

The probability distribution function, $P(x, t)$ of the reaction coordinate x at time t, may be expressed as

$$P(x,t) = \langle \delta\left(x(t) - x\right)\rangle \tag{B.1}$$

where the angular brackets represent an average over the distribution of noise. The equation (B.1) may be differentiated with respect to t, by applying the chain rule as

$$\frac{\mathrm{d}P(x,t)}{\mathrm{d}t} = -\frac{\mathrm{d}}{\mathrm{d}x}\left\langle \delta\left(x(t) - x\right)\frac{\mathrm{d}x(t)}{\mathrm{d}t}\right\rangle. \tag{B.2}$$

By substituting equation (A.7) in the above equation, we get

$$\frac{\mathrm{d}P(x,t)}{\mathrm{d}t} = -\frac{\mathrm{d}}{\mathrm{d}x}\left\langle \delta\left(x(t) - x\right)\left[-\Upsilon(t)x(t) - \frac{1}{k_{\mathrm{S}}}\bar{\xi}(t) + \frac{1}{k_{\mathrm{S}}}\bar{W}(x(t))\right]\right\rangle, \tag{B.3}$$

where,

$$\bar{\xi}(t) = \mathcal{Z}(t)\frac{\mathrm{d}}{\mathrm{d}t}\int_0^t \frac{\phi(t-t')\xi(t')}{\mathcal{Z}(t)}\,\mathrm{d}t', \tag{B.4}$$

and

$$\bar{W}(x(t)) = \mathcal{Z}(t)\frac{\mathrm{d}}{\mathrm{d}t}\int_0^t \frac{\phi(t-t')Wx(t')}{\mathcal{Z}(t)}\,\mathrm{d}t'. \tag{B.5}$$

The solution of equation (B.4) is approximated at short times. Thus, the equation may be rewritten as

$$\bar{W}(x(t)) = \mathcal{Z}(t)\frac{\mathrm{d}}{\mathrm{d}t}\int_0^t \frac{\phi(t')W(x(t-t'))}{\mathcal{Z}(t)}\,\mathrm{d}t', \tag{B.6}$$

Such that $W(x(t-t'))$ may be expanded through the Taylor series, as

$$W(x(t-t')) \approx W(x(t)) - t'W'(x(t))\dot{x}(t) + \frac{t''W''(x(t))\ddot{x}(t)}{2!} + \ldots. \tag{B.7}$$

where W' denotes the differentiation of W with respect to $x(t)$, and keeping only the first term of series as an approximation. The higher order terms comprise the derivatives of W, which requires the estimation of a fraction of two hypergeometric functions that leads to the form of continued fractions [51]. The computation of such fractions is mathematically challenging and is also not exact. Hence, there is a need for such an approximation to discard off the higher order terms which involves the derivatives of W, in order to obtain the analytically closed form solution of the problem. Thus, equation (B.6) becomes

$$\bar{W}(x(t)) = \mathcal{Z}(t)\frac{\mathrm{d}}{\mathrm{d}x}\int_0^t \frac{\phi(t')W(x(t))}{\mathcal{Z}(t)}\,\mathrm{d}t'. \tag{B.8}$$

J. Stat. Mech. (2020) 073411

this equation may be further simplified as

$$\bar{W}(x(t)) = -\frac{W(x(t))}{\mathcal{Z}(t)}\frac{\mathrm{d}\mathcal{Z}(t)}{\mathrm{d}t}. \tag{B.9}$$

By substituting the value of $\bar{W}(x(t))$ in equation (B.3), the equation simplifies to

$$\frac{\mathrm{d}P(x,t)}{\mathrm{d}t} = -\frac{\Upsilon(t)}{k_{\mathrm{S}}}\frac{\mathrm{d}}{\mathrm{d}x}\mathbf{U}'(x)P(x,t) + \frac{1}{k_{\mathrm{S}}}\frac{\mathrm{d}}{\mathrm{d}x}\langle\delta\left(x(t)-x\right)\bar{\xi}(t)\rangle. \tag{B.10}$$

The second term of the above equation is solved by the application of Novikov's theorem [70] on the ensemble average of the random noise, as

$$\langle\delta\left(x(t)-x\right)\bar{\xi}(t)\rangle = -\frac{\mathrm{d}}{\mathrm{d}x}\int_0^t \langle\xi(t)\xi(t')\rangle\langle\delta\left(x(t)-x\right)\frac{\mathrm{d}x(t)}{\mathrm{d}\bar{\xi}(t')}\rangle\,\mathrm{d}t'. \tag{B.11}$$

To estimate $\frac{\mathrm{d}x(t)}{\mathrm{d}\bar{\xi}(t')}$, equation (A.7) may be functionally differentiated with respect to $\bar{\xi}(t')$, to obtain

$$\frac{\mathrm{d}}{\mathrm{d}t}\frac{\mathrm{d}x(t)}{d\bar{\xi}(t')} = -\Upsilon(t)\frac{\mathrm{d}x(t)}{\mathrm{d}\bar{\xi}(t')} - \frac{1}{k_{\mathrm{S}}}\delta(t-t') + \frac{1}{k_{\mathrm{S}}}\Upsilon(t)W'(x(t))\frac{\mathrm{d}x(t)}{\mathrm{d}\bar{\xi}(t')}. \tag{B.12}$$

From the assumption in equation (B.7), the equation becomes

$$\frac{\mathrm{d}}{\mathrm{d}t}\frac{\mathrm{d}x(t)}{\mathrm{d}\bar{\xi}(t')} = -\frac{1}{k_{\mathrm{S}}}H(t-t')\exp\left(-\int_{t'}^{t}\Upsilon(q)\,\mathrm{d}q\right), \tag{B.13}$$

where $H(t-t')$ represents Heaviside step function [51]. Hence, with further simplification the equation (B.11) yields the form

$$\langle\delta\left(x(t)-x\right)\bar{\xi}(t)\rangle = -k_{\mathrm{B}}T\Upsilon(t)\frac{\mathrm{d}}{\mathrm{d}x}P(x,t). \tag{B.14}$$

Substitution of equations (B.10) and (B.14) in equation (B.3) to get the desired form of the effective Fokker–Planck equation as

$$\frac{\mathrm{d}P(x,t)}{\mathrm{d}t} = D(t)\left[\frac{\mathrm{d}^2}{\mathrm{d}x^2}P(x,t) + \frac{1}{k_{\mathrm{B}}T}\frac{\mathrm{d}}{\mathrm{d}x}\mathbf{U}'(x)P(x,t)\right]. \tag{B.15}$$

where, $D(t)$ is the time dependent diffusion coefficient may be represented as $D(t) = -\frac{k_{\mathrm{B}}T}{k_S}\Upsilon(t) = \frac{k_{\mathrm{B}}T}{k_S}\frac{\dot{\mathcal{Z}}(t)}{\mathcal{Z}(t)}$.

Appendix C. Solution of effective Fokker–Planck equation

To obtain the solution of equation (B.15) in terms of $P(x,t)$, we define a function [67] $Q(x,t)$ by

$$P(x,t) = P_{\mathrm{s}}(x)Q(x,t), \tag{C.1}$$

J. Stat. Mech. (2020) 073411

where $P_{\rm s}(x)$ depicts the stationary solution of the EFPE. Such that it satisfies the equation (B.15) as

$$\frac{\mathrm{d}^2}{\mathrm{d}x^2}P_{\rm s}(x) + \frac{1}{k_{\rm B}T}\frac{\mathrm{d}}{\mathrm{d}x}\mathbf{U}'(x)P_{\rm s}(x) = 0. \tag{C.2}$$

Hence, its solution with the incorporation of $\mathbf{U}(x)$ from equation (5), is represented by

$$P_{\rm s}(x) = N\frac{\sqrt{\frac{k_{\rm S}}{k_{\rm B}T}}}{(y_1(A,x))^2}, \tag{C.3}$$

where N denotes the normalization constant defined as $N^{-1} = \int_{-\infty}^{\infty}\frac{1}{(y_1(A,x))^2}\,\mathrm{d}x$ such that $N = \frac{\Gamma\left(\frac{4}{2}+\frac{3}{4}\right)}{\sqrt{2}\Gamma\left(\frac{4}{2}+\frac{1}{4}\right)}$. Since, the introduced function $Q(x,t)$ is related to $P(x,t)$, therefore it should satisfy the equation (B.15). The direct substitution of $Q(x,t)$ satisfies the backward FPE as

$$\frac{\mathrm{d}Q(x,t)}{\mathrm{d}t} = D(t)\left[\frac{\mathrm{d}^2}{\mathrm{d}x^2}Q(x,t) - \frac{1}{k_{\rm B}T}\frac{\mathrm{d}}{\mathrm{d}x}\mathbf{U}'(x)Q(x,t)\right]. \tag{C.4}$$

The variable separable form of each solution in their respective spatial and temporal domain, may be presented as

$$P(x,t) = P_\lambda(x)\ \exp\left(-\int_0^t \lambda D(t')\,\mathrm{d}t'\right). \tag{C.5}$$

Similarly,

$$Q(x,t) = Q_\lambda(x)\ \exp\left(-\int_0^t \lambda D(t')\,\mathrm{d}t'\right). \tag{C.6}$$

These equations are substituted in equations (B.15) and (C.4) respectively, such that they obey the eigenfunction equations, hence may be represented as

$$\left[\frac{\mathrm{d}^2}{\mathrm{d}x^2} + \frac{1}{k_{\rm B}T}\frac{\mathrm{d}}{\mathrm{d}x}\mathbf{U}'(x) + \lambda\right]P_\lambda(x) = 0. \tag{C.7}$$

$$\left[\frac{\mathrm{d}^2}{\mathrm{d}x^2} - \frac{1}{k_{\rm B}T}\frac{\mathrm{d}}{\mathrm{d}x}\mathbf{U}'(x) + \lambda\right]Q_\lambda(x) = 0. \tag{C.8}$$

Simultaneously, solving the above two equations by partial integration and then considering the reflecting boundary condition the coefficient $Q(x,t)$ vanishes. Therefore, it suggests that P_λ and Q_λ form a bi-orthogonal system, that may be presented as

$$\int_{-\infty}^{\infty} P_u(x)Q_v(x)\,\mathrm{d}x = \delta_{u,v}. \tag{C.9}$$

J. Stat. Mech. (2020) 073411

The conditional probability distribution $P(x,t|x_0)$ as the solution of equation (9), subjected to the initial condition $P(x,0)=\delta(x-x_0)$, may be represented as

$$P(x,t|x_0)=\sum_{\lambda}\frac{1}{P_{\rm s}(x_0)}P_\lambda(x)P_\lambda(x_0)\exp\left(-\int_0^t\lambda D(t')\,{\rm d}t'\right). \tag{C.10}$$

$P_\lambda(x)$ is the solution of equation (B.15) in the spatial domain which may be presented in the terms of stationary solution $P_{\rm s}(x)$ and $\psi_\lambda(x)$,

$$P_\lambda(x)=P_{\rm s}^{1/2}(x)\psi_\lambda(x), \tag{C.11}$$

Hence, the substitution of the above equation in equation (C.7) may give the resultant equation after some simplification in terms of $\psi(x)$, that may be represented as

$$\frac{{\rm d}^2}{{\rm d}x^2}\psi_\lambda(x)+\left\{\lambda-\left[\left(\frac{\mathbf{U}'(x)}{2k_{\rm B}T}\right)^2-\frac{\mathbf{U}''(x)}{2k_{\rm B}T}\right]\right\}\psi_\lambda(x)=0. \tag{C.12}$$

Comparing it with the solution of Schrodinger equation [67]

$$\frac{{\rm d}^2}{{\rm d}x^2}\varphi(x)+\left[E-V_{\rm eff}(x)\right]\varphi(x)=0. \tag{C.13}$$

Second part in the curly brackets may relate to the effective potential $V_{\rm eff}$ in the Schrodinger equation. Thus, $V_{\rm eff}(x)$ may be calculated by the substitution of equation (5), as

$$V_{\rm eff}(x)=2\left(\frac{y_1'(A,x)}{y_1(A,x)}\right)^2-\frac{y_1''(A,x)}{y_1(A,x)}. \tag{C.14}$$

Equation (C.12) therefore becomes;

$$\frac{{\rm d}^2}{{\rm d}x^2}\psi_\lambda(x)+\left\{\lambda-\left[2\left(\frac{y_1'(A,x)}{y_1(A,x)}\right)^2-\frac{y_1''(A,x)}{y_1(A,x)}\right]\right\}\psi_\lambda(x)=0. \tag{C.15}$$

Converting the above equation in terms of z such as $z=\sqrt{\frac{k_{\rm S}}{k_{\rm B}T}}\,x$ to make it solvable through the available solution of the Weber equation by Darboux transform [49, 50]. Thus, the above equation may be written as,

$$\frac{{\rm d}^2}{{\rm d}z^2}\psi_\lambda(z)+\left\{\frac{k_{\rm B}T}{k_{\rm S}}\lambda-\left[2\,\frac{k_{\rm B}T}{k_{\rm S}}\left(\frac{y_1'(A,z)}{y_1(A,z)}\right)^2-\left(\frac{z^2}{4}+A\right)\right]\right\}\psi_\lambda(z)=0. \tag{C.16}$$

where, $y_1(A,z)=\exp\left(-\frac{z^2}{4}\right)\,{}_1F_1(A/2+1/4,1/2;z^2/2)$ and the prime denotes differentiation with respect to z. Thus, the eigenfunctions and eigenvalues of the equation may be derived from the Darboux transform method [49, 50], and hence the eigensolutions of the equation may be written in terms of x.

J. Stat. Mech. (2020) 073411

The ground state solution of Schrodinger type equation (C.16), with its eigenvalue $\lambda_0 = 0$ may be given as

$$\psi_0(x) = C_0 \left(\frac{k_S}{k_B T}\right)^{1/4} \frac{1}{y_1(A,x)}. \tag{C.17}$$

and, for the excited states may be represented as;

$$\psi_{n+1}(x) = C_{n+1} \left(\frac{k_B T}{k_S}\right)^{1/4} y_1(A,x) \frac{\mathrm{d}}{\mathrm{d}x} \frac{D_n(x)}{y_1(A,x)}. \tag{C.18}$$

here $D_n(x)$ is the parabolic cylinder function [51, 71], defined as $D_n(x) = 2^{-n/2} \exp(-ax^2/2) H_n(x\sqrt{a})$, $H_n(x)$ denotes the Hermite polynomials [51, 71] with eigenvalue $\lambda_{n+1} = \sqrt{\frac{k_B T}{k_S}} \left(n + A + \frac{1}{2}\right)$; $n = 0,\ 1,\ 2, \ldots$

The solution of equation (C.5) in the temporal domain, may be expressed as

$$\tau(t) = \exp\left(-\lambda_{n+1} \int_0^t D(t')\, \mathrm{d}t'\right) \tag{C.19}$$

Substituting the values of $D(t)$ from equation (7) and λ_{n+1}, we get

$$\tau(t) = \mathcal{Z}(t)^{-\left(n+A+\frac{1}{2}\right)} \tag{C.20}$$

where, $\mathcal{Z}(t)$ may be defined from the equation (8).

Appendix D. Estimation of the normalization constant C_0

The eigenfunction of the ground state i.e. for $\lambda_0 = 0$, is given by the Darboux transform method as

$$\psi_0(x) = C_0 \left(\frac{k_S}{k_B T}\right)^{1/4} \frac{1}{y_1(A,x)}. \tag{D.1}$$

From the normalization condition and converting the resultant equation in terms of variable z, where $z = \sqrt{\frac{k_S}{k_B T}} x$, such that the integral may be solved through the method given by Zheng [49, 72], the solution may be given as

$$\frac{1}{C_0^2} = \int_{-\infty}^{\infty} \frac{1}{(y_1(A,z))^2}\, \mathrm{d}z. \tag{D.2}$$

which may be written as;

$$\frac{1}{C_0^2} = K \int_{-\infty}^{\infty} \frac{\mathrm{d}}{\mathrm{d}z} \frac{D_{-A-1/2}(z) - D_{-A-1/2}(-z)}{2y_1(A,z)}\, \mathrm{d}z. \tag{D.3}$$

where,

J. Stat. Mech. (2020) 073411

$$K = -\frac{1}{\sqrt{\pi}} 2^{A/2-1/4}\Gamma(\frac{A}{2}+\frac{1}{4}).$$

$$\frac{1}{C_0^2} = 2K\,\frac{D_{-A-1/2}(z) - D_{-A-1/2}(-z)}{2y_1(A,z)}\bigg|_0^\infty . \tag{D.4}$$

Thus, at $z \to \infty$, the expression becomes

$$C_0^2 = \frac{\Gamma\left(\frac{A}{2}+\frac{3}{4}\right)}{\sqrt{2}\,\Gamma\left(\frac{A}{2}+\frac{1}{4}\right)}. \tag{D.5}$$

Appendix E. Estimation of the normalization constant C_{n+1}

Eigenfunctions of the other excited states from equation (C.16), is given as

$$\psi_{n+1}(x) = C_{n+1}\left(\frac{k_\mathrm{B}T}{k_\mathrm{S}}\right)^{1/4} y_1(A,x)\,\frac{\mathrm{d}}{\mathrm{d}x}\frac{D_n(x)}{y_1(A,x)}. \tag{E.1}$$

The eigenfunction may also be written in the integral form as

$$\psi_{n+1}(x) = -\lambda_{n+1}C_{n+1}\frac{1}{y_1(A,x)}\int_0^x y_1(A,x')D_n(x')\,\mathrm{d}x'. \tag{E.2}$$

Writing this expression in terms of variable z, where $z = \sqrt{\frac{k_\mathrm{S}}{k_\mathrm{B}T}}\,x$, with the normalization condition we get

$$\frac{1}{C_{n+1}^2} = \int_{-\infty}^{\infty} y_1(A,z)\frac{\mathrm{d}}{\mathrm{d}z}\frac{D_n(z)}{y_1(A,z)}\left[-\lambda_{n+1}\frac{1}{y_1(A,z)}\int_0^{z/\sqrt{k_\mathrm{S}/k_\mathrm{B}T}} y_1(A,z')D_n(z')\,\mathrm{d}z'\right]\mathrm{d}z, \tag{E.3}$$

which may be simplified to

$$\frac{1}{C_{n+1}^2} = -\lambda_{n+1}\left[-D_n(z)\frac{y_1(A,z)}{\lambda_{n+1}}\frac{\mathrm{d}}{\mathrm{d}z}\frac{D_n(z)}{y_1(A,z)}\bigg|_{-\infty}^{\infty} - \int_{-\infty}^{\infty}\left(D_n(z')\right)^2\mathrm{d}z'\right], \tag{E.4}$$

that may be written as

$$\frac{1}{C_{n+1}^2} = \sqrt{2\pi}n!\lambda_{n+1}. \tag{E.5}$$

Hence,

$$C_{n+1}^{-2} = \sqrt{2\pi}n!(n+A+\frac{1}{2})\,;\quad n \geqslant 0 \tag{E.6}$$

J. Stat. Mech. (2020) 073411

Appendix F. Derivation of distribution of FPT, $\mathcal{F}(x_0, t)$ in confined domain

The first passage time distribution [56, 67, 73] (FPTD) for each transitions may be evaluated as the moment of first passage times which is obtained by solving the EFPE defined by equation (9). The solution of the EFPE may be addressed in the form of the conditional probability distribution function $P(x, t|x_0)$, which denotes the probability of finding the reaction coordinate, x, at time t, provided the transition trajectory commences at x_0 at time $t = 0$. The two boundaries are considered to be situated in between the zipped state, (x_A) and the transition state, (x_B) or the unzipped, (x_B) via (i) and (ii). The probability of the transitions is defined within the confined domain only. Thus, for the $x_A \leqslant x \leqslant x_B/x_C$, the initial condition of $P(x, t|x_0)$ that satisfy the EFPE, may be defined as

$$P(x, |x_0) = \delta(x - x_0) \tag{F.1}$$

where, $P(x, t|x_0) = 0$ for $x < x_A$ and $x > x_B/x_C$.

Under these conditions, the probability $G(x_0, t)$ of the trajectories which start from x_0 and have not reached at either of the boundaries upto time t, may be expressed as

$$G(x_0, t) = \int_{x_A}^{x_B/x_C} P(x, t|x_0)\, \mathrm{d}x \tag{F.2}$$

The system is homogeneous in time, thus, it follows

$$P(x, t|x_0) = P(x, 0|x_0, -t) \tag{F.3}$$

The probability of those trajectories which manage to reach any one of the boundaries in the confined domain for the first time, in the given time interval $(t, t + \mathrm{d}t)$, may be given as [67]

$$-\,\mathrm{d}G(x_0, t) \equiv G(x_0, t + \mathrm{d}t) - G(x_0, t) \tag{F.4}$$

The distribution function of the first passage time, $\mathcal{F}(x_0, t)$ from equations (F.2) and (F.4) is represented by [56, 67, 73]

$$\mathcal{F}(x_0, t) = -\frac{\mathrm{d}G(x_0, t)}{\mathrm{d}t} = -\frac{\mathrm{d}}{\mathrm{d}t}\int_{x_A}^{x_B/x_C} P(x, t|x_0)\, \mathrm{d}x \tag{F.5}$$

References

[1] Woodside M T, Behnke-Parks W M, Larizadeh K, Travers K, Herschlag D and Block S M 2006 Nanomechanical measurements of the sequence-dependent folding landscapes of single nucleic acid hairpins *Proc. Natl Acad. Sci. USA* **103** 6190–5

[2] Swadling J B, Ishii K, Tahara T and Kitao A 2018 Origins of biological function in DNA and RNA hairpin loop motifs from replica exchange molecular dynamics simulation *Phys. Chem. Chem. Phys.* **20** 2990–3001

[3] Varani G 1995 Exceptionally stable nucleic acid hairpins *Annu. Rev. Biophys. Biomol. Struct.* **24** 379–404

[4] Glucksmann-Kuis M A, Dai X, Markiewicz P and Rothman-Denes L B 1996 E coli SSB activates N4 virion RNA polymerase promoters by stabilizing a DNA hairpin required for promoter recognition *Cell* **84** 147–54

J. Stat. Mech. (2020) 073411

[5] Mishra G, Giri D, Li M and Kumar S 2011 Role of loop entropy in the force induced melting of DNA hairpin *J. Chem. Phys.* **135** 07B611
[6] Singh A R, Giri D and Kumar S 2010 Force induced melting of the constrained DNA *J. Chem. Phys.* **132** 06B611
[7] Lin M M, Meinhold L, Shorokhov D and Zewail A H 2008 Unfolding and melting of DNA (RNA) hairpins: the concept of structure-specific 2D dynamic landscapes *Phys. Chem. Chem. Phys.* **10** 4227–39
[8] Bustamante C, Bryant Z and Smith S B 2003 Ten years of tension: single-molecule DNA mechanics *Nature* **421** 423
[9] Rief M, Clausen-Schaumann H and Gaub H E 1999 Sequence-dependent mechanics of single DNA molecules *Nat. Struct. Mol. Biol.* **6** 346
[10] Cluzel P, Lebrun A, Heller C, Lavery R, Viovy J-L, Chatenay D and Caron F 1996 DNA: an extensible molecule *Science* **271** 792–4
[11] Rief M, Oesterhelt F, Heymann B and Gaub H E 1997 Single molecule force spectroscopy on polysaccharides by atomic force microscopy *Science* **275** 1295–7
[12] Tskhovrebova L, Trinick J, Sleep J and Simmons R 1997 Elasticity and unfolding of single molecules of the giant muscle protein titin *Nature* **387** 308
[13] Merkel R, Nassoy P, Leung A, Ritchie K and Evans E 1999 Energy landscapes of receptor–ligand bonds explored with dynamic force spectroscopy *Nature* **397** 50
[14] Kellermayer M S, Smith S B, Granzier H L and Bustamante C 1997 Folding–unfolding transitions in single titin molecules characterized with laser tweezers *Science* **276** 1112–6
[15] Smith S B, Cui Y and Bustamante C 2003 [7] Optical-trap force transducer that operates by direct measurement of light momentum **361** 134–62
[16] Woodside M T, Anthony P C, Behnke-Parks W M, Larizadeh K, Herschlag D and Block S M 2006 Direct measurement of the full, sequence-dependent folding landscape of a nucleic acid *Science* **314** 1001–4
[17] Gupta A N, Vincent A, Neupane K, Yu H, Wang F and Woodside M T 2011 Experimental validation of free-energy-landscape reconstruction from non-equilibrium single-molecule force spectroscopy measurements *Nat. Phys.* **7** 631
[18] Engel M C, Ritchie D B, Foster D A, Beach K S and Woodside M T 2014 Reconstructing folding energy landscape profiles from non-equilibrium pulling curves with an inverse Weierstrass integral transform *Phys. Rev. Lett.* **113** 238104
[19] Neupane K, Ritchie D B, Yu H, Foster D A, Wang F and Woodside M T 2012 Transition path times for nucleic acid folding determined from energy-landscape analysis of single-molecule trajectories *Phys. Rev. Lett.* **109** 068102
[20] Vandebroek H and Vanderzande C 2017 The effect of active fluctuations on the dynamics of particles, motors and DNA-hairpins *Soft Matter* **13** 2181–91
[21] Preus S and Wilhelmsson L M 2012 Advances in quantitative FRET-based methods for studying nucleic acids *ChemBioChem* **13** 1990–2001
[22] Ruedas-Rama M, Alvarez-Pez J and Orte A 2013 Solving single biomolecules by advanced FRET-based single-molecule fluorescence techniques *Biophys. Rev. Lett.* **8** 161–90
[23] Juette M F, Terry D S, Wasserman M R, Altman R B, Zhou Z, Zhao H and Blanchard S C 2016 Single-molecule imaging of non-equilibrium molecular ensembles on the millisecond timescale *Nat. Methods* **13** 341
[24] Woodside M T, García-García C and Block S M 2008 Folding and unfolding single RNA molecules under tension *Curr. Opin. Chem. Biol.* **12** 640–6
[25] Žoldák G and Rief M 2013 Force as a single molecule probe of multidimensional protein energy landscapes *Curr. Opin. Struct. Biol.* **23** 48–57
[26] Greenleaf W J, Woodside M T and Block S M 2007 High-resolution, single-molecule measurements of biomolecular motion *Annu. Rev. Biophys. Biomol. Struct.* **36** 171–90
[27] McCluskey K, Shaw E, Lafontaine D A and Penedo J C 2014 Single-molecule fluorescence of nucleic acids *Fluorescence Spectroscopy and Microscopy* (Berlin: Springer) pp 759–91
[28] Lang M J, Fordyce P M, Engh A M, Neuman K C and Block S M 2004 Simultaneous, coincident optical trapping and single-molecule fluorescence *Nat. Methods* **1** 133
[29] Neupane K, Wang F and Woodside M T 2017 Direct measurement of sequence-dependent transition path times and conformational diffusion in DNA duplex formation *Proc. Natl Acad. Sci.* **114** 1329–34
[30] Hummer G and Eaton W A 2012 Transition path times for DNA and RNA folding from force spectroscopy *Physics* **5** 87
[31] Laleman M, Carlon E and Orland H 2017 Transition path time distributions *J. Chem. Phys.* **147** 214103
[32] Caraglio M, Put S, Carlon E and Vanderzande C 2018 The influence of absorbing boundary conditions on the transition path time statistics *Phys. Chem. Chem. Phys.* **20** 25676–82

[33] Chaudhury S and Makarov D E 2010 A harmonic transition state approximation for the duration of reactive events in complex molecular rearrangements *J. Chem. Phys.* **133** 034118
[34] Carlon E, Orland H, Sakaue T and Vanderzande C 2018 Effect of memory and active forces on transition path time distributions *J. Phys. Chem* B **122** 11186–94
[35] Frederickx R, Carlon E *et al* 2014 Anomalous dynamics of DNA hairpin folding *Phys. Rev. Lett.* **112** 198102
[36] Pyo A G and Woodside M T 2019 Memory effects in single-molecule force spectroscopy measurements of biomolecular folding *Phys. Chem. Chem. Phys.* **21** 24527–34
[37] Pollak E 2016 Transition path time distribution and the transition path free energy barrier *Phys. Chem. Chem. Phys.* **18** 28872–82
[38] Sakaue T, Walter J-C, Carlon E and Vanderzande C 2017 Non-Markovian dynamics of reaction coordinate in polymer folding *Soft Matter* **13** 3174–81
[39] Satija R and Makarov D E 2019 Generalized Langevin equation as a model for barrier crossing dynamics in biomolecular folding *J. Phys. Chem* B **123** 802–10
[40] Neupane K, Manuel A P, Lambert J and Woodside M T 2015 Transition-path probability as a test of reaction-coordinate quality reveals DNA hairpin folding is a one-dimensional diffusive process *J. Phys. Chem. Lett.* **6** 1005–10
[41] Berezhkovskii A and Szabo A 2005 One-dimensional reaction coordinates for diffusive activated rate processes in many dimensions *J. Chem. Phys.* **122** 014503
[42] Manuel A P, Lambert J and Woodside M T 2015 Reconstructing folding energy landscapes from splitting probability analysis of single-molecule trajectories *Proc. Natl Acad. Sci. USA* **112** 7183–8
[43] Neupane K, Foster D A, Dee D R, Yu H, Wang F and Woodside M T 2016 Direct observation of transition paths during the folding of proteins and nucleic acids *Science* **352** 239–42
[44] Zwanzig R 2001 *Non-equilibrium Statistical Mechanics* (Oxford: Oxford University Press)
[45] Kubo R, Toda M and Hashitsume N 2012 *Statistical Physics II: Nonequilibrium Statistical Mechanics* vol 31 (Berlin: Springer)
[46] Lin J-C and Thirumalai D 2008 Relative stability of helices determines the folding landscape of adenine riboswitch aptamers *J. Am. Chem. Soc.* **130** 14080–1
[47] Sharma S and Biswas P 2017 Hydration water dynamics around a protein surface: a first passage time approach *J. Phys. Condens. Matter* **30** 035101
[48] Sharma S and Biswas P 2019 Unusual dynamics of hydration water around motor proteins with long-ranged hydrodynamic fluctuations *Physica* A 122045
[49] Zheng W 1984 The Darboux transformation and solvable double-well potential models for Schrödinger equations *J. Math. Phys.* **25** 88–90
[50] Mondescu R P and Muthukumar M 1999 Statistics of an ideal polymer in a multistable potential: exact solutions and instanton approximation *J. Chem. Phys.* **110** 12240–9
[51] Abramowitz M and Stegun I A 1965 *Handbook of Mathematical Functions: With Formulas, Graphs, and Mathematical Tables* (New York: Dover Publications)
[52] Buchholz H 2013 *The Confluent Hypergeometric Function: With Special Emphasis on its Applications* vol 15 (Berlin: Springer Science & Business Media)
[53] Gorenflo R and Kilbas A 2016 *Mittag-Leffler Functions, Related Topics and Applications* (Berlin: Springer)
[54] Fox R F 1986 Uniform convergence to an effective Fokker–Planck equation for weakly colored noise *Phys. Rev.* A **34** 4525
[55] Fox R F 1986 Functional-calculus approach to stochastic differential equations *Phys. Rev.* A **33** 467
[56] Redner S 2001 *A Guide to First-Passage Processes* (Cambridge: Cambridge University Press)
[57] Sanders L P and Ambjörnsson T 2012 First passage times for a tracer particle in single file diffusion and fractional Brownian motion *J. Chem. Phys.* **136** 05B605
[58] Manghi M and Destainville N 2016 Physics of base-pairing dynamics in DNA *Phys. Rep.* **631** 1–41
[59] Daldrop J O, Kim W K and Netz R R 2016 Transition paths are hot *Europhys. Lett.* **113** 18004
[60] Imparato A, Sbrana F and Vassalli M 2008 Reconstructing the free-energy landscape of a polyprotein by single-molecule experiments *Europhys. Lett.* **82** 58006
[61] Mossa A, Manosas M, Forns N, Huguet J M and Ritort F 2009 Dynamic force spectroscopy of DNA hairpins: I. Force kinetics and free energy landscapes *J. Stat. Mech.: Theory Exp* **2009** P02060
[62] Li P T, Collin D, Smith S B, Bustamante C and Tinoco I Jr 2006 Probing the mechanical folding kinetics of tar RNA by hopping, force-jump, and force-ramp methods *Biophys. J.* **90** 250–60
[63] Cocco S, Marko J F and Monasson R 2002 Theoretical models for single-molecule DNA and RNA experiments: from elasticity to unzipping *C. R. Phys.* **3** 569–84
[64] Ansari A and Kuznetsov S V 2005 Is hairpin formation in single-stranded polynucleotide diffusion-controlled? *J. Phys. Chem* B **109** 12982–9

J. Stat. Mech. (2020) 073411

[65] Nam G-M and Makarov D E 2016 Extracting intrinsic dynamic parameters of biomolecular folding from single-molecule force spectroscopy experiments *Protein Sci.* **25** 123–34
[66] Kim W K and Netz R R 2015 The mean shape of transition and first-passage paths *J. Chem. Phys.* **143** 224108
[67] Gardiner C W 1985 *Handbook of Stochastic Methods* vol 3 (Berlin: Springer)
[68] Berezhkovskii A M, Dagdug L and Bezrukov S M 2017 Mean direct-transit and looping times as functions of the potential shape *J. Phys. Chem* B **121** 5455–60
[69] Medina E, Satija R and Makarov D E 2018 Transition path times in non-Markovian activated rate processes *J. Phys. Chem* B **122** 11400–13
[70] Novikov E A 1965 Functionals and the random-force method in turbulence theory *Sov. Phys. JETP* **20** 1290–4
[71] Gradshteyn I S and Ryzhik I M 2014 *Table of Integrals, Series, and Products* (New York: Academic)
[72] Hongler M-O and Zheng W 1983 Exact results for the diffusion in a class of asymmetric bistable potentials *J. Math. Phys.* **24** 336–40
[73] Risken H 1996 *The Fokker-Planck Equation* (Berlin: Springer)

J. Stat. Mech. (2020) 073411